NUMERICAL STUDY OF FLOW AND HEAT TRANSFER CHARACTERISTICS OF BACKWARD-FACING STEP USING NANOFLUID

Mohamed BOUAZIZ[1], Lotfi BOUAZIZI[2]*, Said TURKI[3]

A numerical investigation was conducted to analyze the effect of buoyancy forces on the flow field and heat transfer over a backward-facing step using copper-water nanofluid. The flow behind the primary recirculation zone was found to be unsteady when Ri exceeded the values of Ri_{cr} = 0.85, 1.15, 1.55, 2.05 and 2.55 for φ = 0%, 5%, 10%, 15% and 20% respectively. The reattachment length Lr decreases when φ increases and correlations between Lr and Ri were obtained for different φ. A discussion about the buoyancy effect on the heat transfer exchanged between the horizontal walls is presented for different φ.

Keywords: Cu – water nanofluid, backward-facing step, mixed convection, heat transfer, buoyancy forces.

1. Introduction

It is well known that the study of backward-facing step flows is an important branch of fundamental fluid mechanics. Since the publication of Armaly's et al. [1] work using pure fluid, several studies have been conducted in this area such as those of Kim and Moin [2], Gartling [3], Barkeley et al. [4], Abu-Mulaweh [5], Ramsak and Skerg [6], Tinney and Ukeiley [7] among others... However, to the best of our knowledge, few research studies have tackled this area using nanofluids. This new class of fluids, composed of metal nanoparticles suspended in a base fluid, has recently appeared, due to their anomalous thermal conductivity enhancement and many studies [8-14] have been undertaken in the area of flow and heat transfer of nanofluids, showing that these new fluids have a remarkable power of heat exchange compared to conventional liquid. This enhanced thermal behavior of nanofluids could provide a basis for an enormous innovation for heat transfer intensification, which is a major importance to a number of industrial sectors including transportation, power generation, heating, cooling, ventilation and air-conditioning, ... etc. Concerning the flow of nanofluids over a backward-facing step, Abu-Nada [15] was notably the pioneer to analyze the effect

[1] National Engineering School of Sfax, Tunisia, email: abou2m@gmail.com
[2]* National Engineering School of Sfax, Tunisia, email: lot.bouazizi@yahoo.fr
[3] National Engineering School of Sfax, Tunisia, email: said.turki@fss.rnu.tn

of nanofluids on the flow pattern and its related heat transfer. Results, obtained in forced convection, show that nanoparticles with high thermal conductivity have more enhancement on the value of Nusselt number outside the recirculation zones. However, within the primary and secondary recirculation zones, nanoparticles with low thermal conductivity have a better enhancement of heat transfer. Al-aswadi et al. [16] studied numerically the laminar forced convection flow over a backward-facing step in a duct using different types of nanoparticles (*Au, Ag, Al_2O_3, Cu, CuO, diamond, SiO_2* and *TiO_2*) dispersed in a base fluid (*water*). They reported that the recirculation size and reattachment length increase as the Reynolds number increases. Furthermore, they showed that nanofluids with low dense nanoparticles, such as *SiO_2*, have a higher velocity than those with high dense nanoparticles, such as *Au*. The effect of nanofluids flow on a mixed convection heat transfer over a 2D horizontal micro scale backward-facing step placed in a duct has been conducted numerically by Kherbeet et al. [17]. Their results, obtained for different nanoparticles (*Al_2O_3, CuO, SiO_2* and *ZnO*) with volume fractions in the range of 1–4% and nanoparticles diameter ranging from 25nm to 70nm, show that the Nusselt number increases with the increase of the volume fraction and Reynolds number. Furthermore, the nanofluid of *SiO_2* nanoparticles was observed to have the highest Nusselt number value. They also found that the Nusselt number increases with the decrease of the nanoparticle diameter. However, there is no recirculation region observed at the step and along the duct. Mohammed et al. [18-19] studied the influence of nanofluids on mixed convective heat transfer over horizontal and vertical backward-facing steps. Their results obtained for different types of nanoparticles (*Ag, Al_2O_3, Au, Cu, CuO, diamond, SiO_2*, and *TiO_2*) with 5% volume fraction, show that nanofluids without secondary recirculation region have a higher Nusselt number which increases with the decrease in Prandtl number. Furthermore, they found that the diamond-water nanofluid in the primary recirculation region has the highest Nusselt number, while *SiO_2-water* nanofluid has the highest Nusselt number downstream of the primary recirculation region. Saffari and Gandjalikhan [20] studied the laminar forced convection flow of nanofluids over a 2D horizontal backward-facing step under bleeding condition. They deduced that the recirculation zones and the reattachment length increase as the bleeding coefficient increases. They also showed that the Nusselt number and the friction coefficient increase as volume fraction increases.

The present research work was carried out to contribute to the existing knowledge of backward-facing step flow using *Cu-water* nanofluid. It is a numerical investigation on mixed convection flow over a backward-facing step. The study is particularly focused on the effect of both buoyancy term (Richardson number) and the nanoparticles volume fraction on the flow pattern and its related heat transfer. Numerical simulations are performed out for Richardson number *Ri*

up to 2.85 and a volume fraction φ of Copper nanoparticles from 0 to 20% at a fixed Reynolds number $Re = 450$ and Prandtl number Pr=6.2.

2. Governing equations

Both of the flow geometry and the coordinate system are shown in Fig. 1. The conservation equations describing the flow are time-dependent, two-dimensional Navier-Stokes and energy equations of incompressible nanofluid. The base fluid (*water*) and the nanoparticles (*Cu*) are assumed to be in thermal equilibrium and all the physical properties of nanofluids (Table 1) are assumed to be constant except for the variation of density in buoyancy term of momentum equation. The density variation is treated by the Boussinesq approximation. Thus, the dimensionless of the continuity, momentum and thermal energy equations governing the laminar flow over the backward-facing step can be written in the following conservative form:

$$div(\boldsymbol{V}) = 0 \tag{1}$$

$$\frac{\partial u}{\partial \tau} + div(\boldsymbol{J_u}) = -\frac{\rho_f}{\rho_{nf}}\frac{\partial P}{\partial x}, \qquad \boldsymbol{J}_u = u\boldsymbol{V} - \frac{1}{Re}\frac{\mu_{nf}}{\mu_f}\frac{\rho_f}{\rho_{nf}}\boldsymbol{grad}(u) \tag{2}$$

$$\frac{\partial v}{\partial \tau} + div(\boldsymbol{J_v}) = -\frac{\rho_f}{\rho_{nf}}\frac{\partial P}{\partial y} + \frac{\varphi\rho_s\beta_s + (1-\varphi)\rho_f\beta_f}{\rho_{nf}\beta_f} Ri\theta,$$

$$\boldsymbol{J}_v = v\boldsymbol{V} - \frac{1}{Re}\frac{\mu_{nf}}{\mu_f}\frac{\rho_f}{\rho_{nf}}\boldsymbol{grad}(v) \tag{3}$$

$$\frac{\partial \theta}{\partial \tau} + div(\boldsymbol{J_\theta}) = 0, \qquad \boldsymbol{J}_\theta = \theta\boldsymbol{V} - \frac{1}{Re.Pr}\frac{\alpha_{nf}}{\alpha_f}\boldsymbol{grad}(\theta) \tag{4}$$

where ρ, β, μ, α and φ are the density, the coefficient of thermal expansion, the dynamic viscosity, the thermal diffusivity and the nanoparticles volume fraction, respectively, taking into account subscripts *f* for fluid, *s* for solid and *nf* for nanofluid.

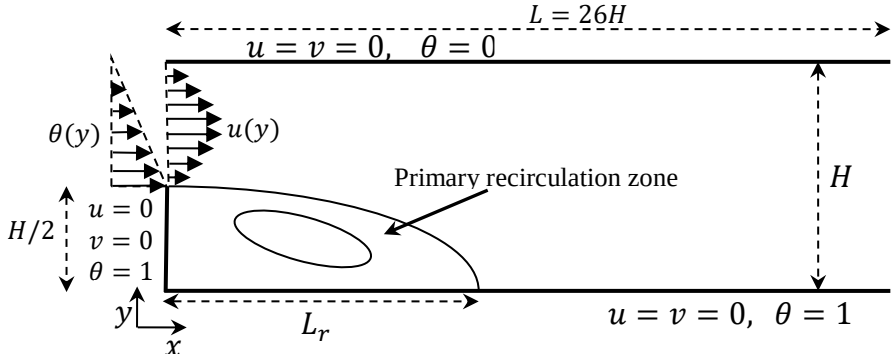

Fig. 1. Configuration definition

In the above equations, the space coordinates; velocities, time and pressure are normalized with the downstream channel height *H*, the maximum velocity of

the channel inlet u_0, the characteristic time H/u_0 and the characteristic pressure $\rho_f u_0^2$ respectively. The dimensionless variable θ was defined as: $\theta = (T-T_c)/(T_h-T_c)$ where T_h and T_c are hot and cold temperatures respectively.

Table 1

Thermo-physical properties

Property	Fluid phase (Water)	Cu
Cp (J/kg K)	4179	385
ρ (kg/m^3	997.1	8933
k (W/m K)	0.613	400
$\alpha \times 10^7$ (m^2/s)	1.47	1163.1

In equations (2) - (4), the viscosity of the nanofluid is given by Brinkman [21] as follows:

$$\mu_{nf} = \mu_f / (1- \varphi)^{2.5} \quad (5)$$

The thermal diffusivity of the nanofluid is defined as follows:

$$\alpha_{nf} = k_{nf} /(\rho c_p)_{nf} \quad (6)$$

where the conductivity of the nanofluid k_{nf} is expressed as (Khanafer et al. [22]):

$$k_{nf}/k_f = [k_s+2k_f-2\varphi(k_f- k_s)]/[k_s+2k_f+\varphi(k_f- k_s)] \quad (7)$$

The effective density ρ_{nf} and the heat capacitance $(\rho c_p)_{nf}$ of the nanofluid are expressed as (Xuan and Li [8]):

$$\rho_{nf} = (1- \varphi) \rho_f + \varphi\rho_s \quad (8)$$

$$(\rho c_p)_{nf} = (1- \varphi) (\rho c_p)_f + \varphi(\rho c_p)_s \quad (9)$$

The Reynolds number *Re*, the Richardson number *Ri* and the Prandtl number *Pr* are defined as follows:

$$Re = \rho_f u_0 H /\mu_f \qquad Ri = g \beta_f H^3/\nu_f^2 Re^2 \qquad Pr = \nu_f /\alpha_f \quad (10)$$

where ν_f is the kinematic viscosity of the base fluid.

No-slip boundary conditions for velocities on all the solid walls were used. The temperature at the upper wall of the channel is constant and equal to T_c, corresponding to $\theta = 0$. The step and the lower walls of the channel are assumed to be isothermally heated at T_h, corresponding to $\theta = 1$.

At the channel inlet, a normal component of velocity is assumed to be zero and a fully developed parabolic profile for the axial velocity, expressed by $u(y)=-16(y^2-1.5y+0.5)$, is deployed. The temperature of the incoming stream is assumed to be linear and expressed by [15] $\theta(y) = 2(1-y)$.

At the channel exit, the convective boundary condition, given by $\partial\phi/\partial t + u_{av} \partial\phi/\partial x = 0$, is used where the variable ϕ is the dependent variable (u, v,θ) and u_{av} is the mean channel inlet velocity. It is noted here that, as mentioned by Sohankar et al. [23] and Abbassi et al. [24], the convective boundary condition reduces the number of iterations per time step and allows a shorter downstream computational domain when compared to the case of the Neumann boundary condition.

The thermal heat flux exchanged between the flow and the horizontal walls is characterized by the space averaged Nusselt number evaluated as follows:

$$Nu_{av} = \frac{1}{L}\int_0^L Nu(x)dx \quad (11)$$

Where $Nu(x)$ is the local Nusselt number, computed with the following equation (Abu-Nada [15]):

$$Nu(x) = \frac{1}{\theta_b(x)-1}\frac{k_{nf}}{k_f}\frac{\partial\theta}{\partial y}\Big|_{wall} \quad (12)$$

$\theta_b(x)$ is the bulk temperature, calculated using the velocity and the temperature distribution with the equation:

$$\theta_b(x) = \frac{\int_0^1 u\theta dy}{\int_0^1 u dy} \quad (13)$$

3. Solution procedures

The combined continuity, momentum and energy equations are solved using a finite volume method of Patankar [25], where the control volume cells for velocity components are staggered with respect to the main control volume cells. This use of a staggered grid prevents the occurrence of checkerboard pressure fields. The convection and the diffusion terms in equations (2-4) were discretized using central differences of second order accuracy. The SIMPLER algorithm was applied to solve the pressure-velocity coupling in conjunction with an alternating direction implicit scheme to perform the time evolution. The numerical simulations were done using a specific code developed by Turki and Lauriat [26] to study the natural and the mixed convection of non-Newtonian fluids, that was adapted and modified to the present problem.

Our computations were achieved using 366x119 non uniform meshes with a variable grid sizes $10^{-2} \leq \Delta x \leq 10^{-1}$ and $10^{-3} \leq \Delta y \leq 10^{-2}$. In order to study the grid independence, one case was run with 561x255 grid points with $5.10^{-3} \leq \Delta x \leq 7.10^{-2}$ and $5.10^{-4} \leq \Delta y \leq 5.10^{-3}$ for $Re = 450$, $Pr = 6.2$, $Ri = 0$ and $\varphi = 0$ (pure water). The computation results show a difference of only 1.5%, 0.7% and 1.1% in the values of the reattachment length Lr, the space average Nusselt numbers Nu_{av} at the lower and the upper walls of the channel respectively. Since the computation time with 561x255 grids is nearly four times higher than that with 366x119 grids, we decided to cancel it and carry out that of the 366x119 grids.

The present computational procedure has been validated by comparing the predicted reattachment length and averaged Nusselt number with the results of Abu-Nada [15] obtained in laminar forced convection flow of *Cu-water* nanofluid over a backward-facing step. Figures 2 and 3 show that the present results, obtained with 366x119 non uniform grids, are in good agreement with those found by Abu-Nada. The maximum deviations are of only about 3% and 2.7% for the reattachment length and the averaged Nusselt number respectively. We can therefore conclude

that our computational code can predict correctly the flow and heat transfer of *Cu-water* nanofluid over a backward-facing step.

For all the investigated cases in this paper, the computational time step used is equal to $\Delta\tau = 0.005$. A time step of $\Delta\tau = 0.0025$ does not cause any change on the numerical results.

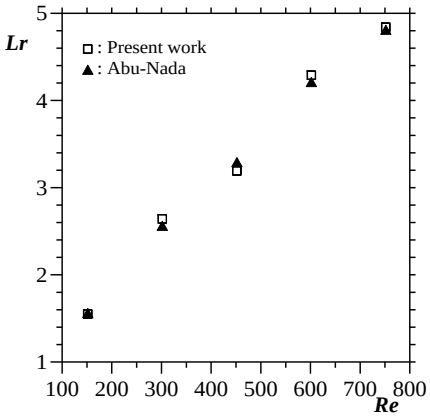

Fig. 2. Comparison of reattachment length results with those obtained by Abu-Nada [15]

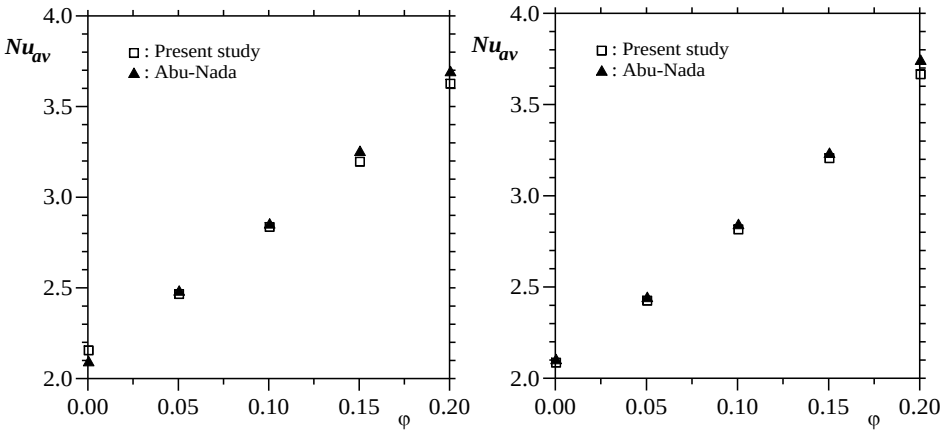

(a): Lower wall (b): Upper wall

Fig. 3. Comparison of space-averaged Nusselt number results with those obtained by Abu-Nada [15] at $Re = 450$

4. Results and discussion

Computations were carried out for a *Cu-water* nanofluid flow over a backward-facing step under buoyancy parameter *Ri* up to 2.85, volume fraction φ ranging from 0 to 0.2 when the Reynolds number and the Prandtl number are kept constant at $Re = 450$ and Pr=6.2 respectively.

Figure 4 shows the instantaneous streamlines for two Richardson numbers (Ri=1 and Ri=2) at φ = 10%. In the region behind the primary recirculation zone, the flow is seen to be steady at Ri = 1 where all the streamlines are found parallel.

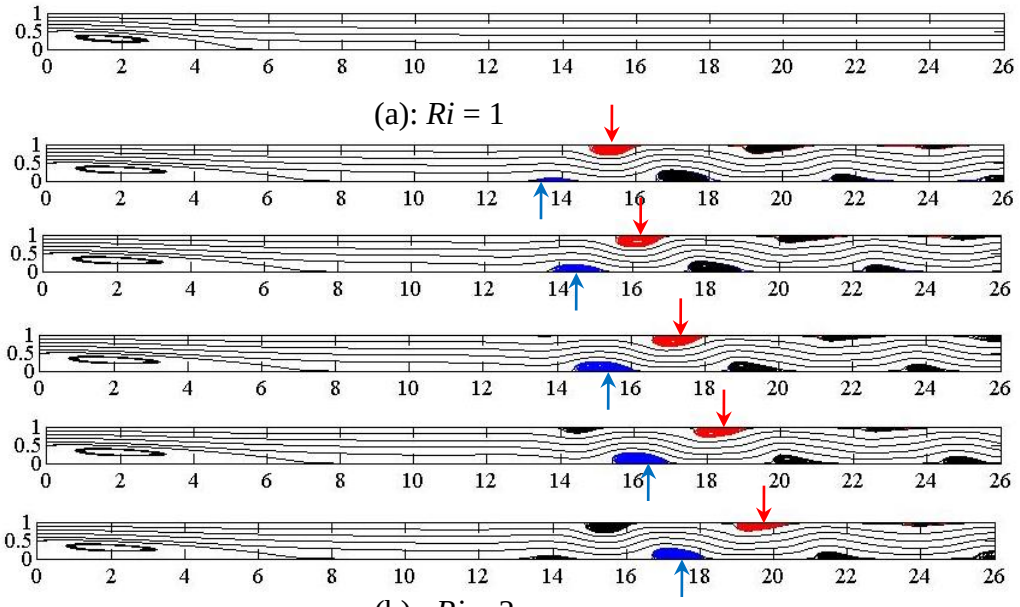

(a): Ri = 1

(b) : Ri = 2

Fig. 4. Flow pattern for two Richardson numbers at φ = 10%

For Ri = 2, a remarkable change in the flow pattern was observed where an oscillatory nature of the flow downstream the primary recirculation zone could be seen clearly in the streamlines. In fact, this behavior is due to the presence of convective cells which are created near the horizontal walls and which move in the direction of the main flow. Indeed, by presenting the temporal variation of the the space averaged Nusselt number Nu_{av} on the horizontal walls, as shown in Fig. 5, it is clear that the oscillatory nature of Nu_{av} means the movement of cells near the horizontal walls. The reason of the occurrence of the convective cells may be caused by the depression zones created by the buoyancy forces once they play a major role. Starting from Ri = 1 and relying on the flow visualization by slowly increasing the Richardson number, the main flow becomes unsteady and oscillatory once it exceeds a critical value which is found approximately equal to Ri_{cr}=1.55. For volume fraction φ ranging from 0% to 20%, numerical results reported in Fig. 6 show that the critical Richardson number Ri_{cr} characterizing the onset of convective cells near the horizontal walls increases with increasing the volume fraction. This can be explained by the increase of the dynamic viscosity of the nanofluid with the increase of φ (see equation 5) and hence the friction forces on the horizontal walls increase. These forces tend to oppose to the formation of the convective cells delaying therefore the transition to the oscillatory flow regime. Referring back to

Fig. 6 again, it can be seen that Ri_{cr} varies linearly with respect to the volume fraction φ of suspended particles over the range of 0%-20%. A least-square method was used to get a linear fit on a plot of Ri_{cr} versus φ and the following expression may be derived:

$$Ri_{cr} = 8.6\ \varphi + 0.8 \quad (14)$$

This correlation has a maximum deviation of the order of 3.8% with the computed results. In addition, the curve given by this correlation separates the diagram presented in Fig. 6 into two areas allowing to define the behavior of the flow behind the primary recirculation zone for a given couple (φ, Ri).

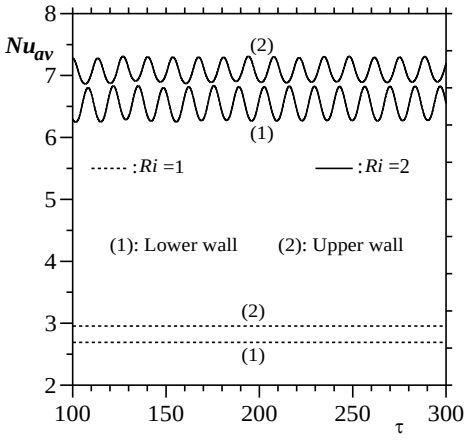

Fig. 5. Variation of the space -averaged Nusselt number with time for two Richardson numbers (φ = 10%)

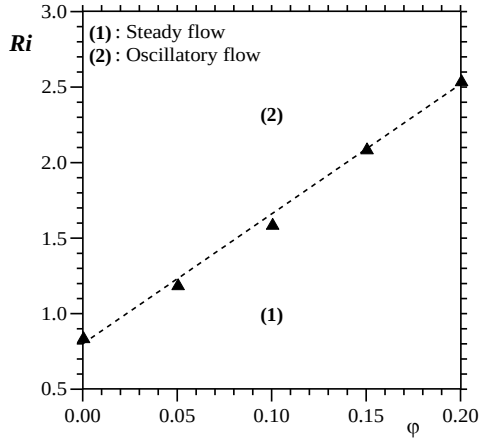

Fig. 6. Diagram defining the different flow regimes behind the primary recirculation zone (▲: Numerical results of Ri_{cr} -----: empirical correlation)

By slowly increasing the Richardson number from Ri_{cr} again, the numerical results have shown that the onset of the convective cells approach to the primary recirculation zone, as illustrated in Fig.7. When Ri exceeds approximately the values of Ri_l = 1.1, 1.55, 2, 2.4 and 2.85 for φ = 0%, 5%, 10%, 15% and 20%, respectively, and contrarily to what was observed for $R_i \leq Ri_l$, where Lr remains constant in time at a given couple (φ, Ri), a variation in time of the primary recirculation zone size was noted. This behavior may be caused by the generation of a small vortex located at the tip of the primary recirculation zone as shown in Fig. 8. This vortex which grows in size with time leaves the primary recirculation zone toward the main flow. This causes oscillation in the size of the primary recirculation zone, and hence oscillation of the reattachment length, as shown in Fig. 9.

In what follows, our study is limited to the flow of *Cu-water* nanofluid corresponding to $Ri \leq Ri_l$. Our focus is to analyze the effect of the buoyancy forces as well as the volume fraction of the suspended nanoparticles on the reattachment

length *Lr* and the heat flux exchanged between the horizontal walls and the flow. Figure 10 displays the variation of the reattachment length with Richardson number

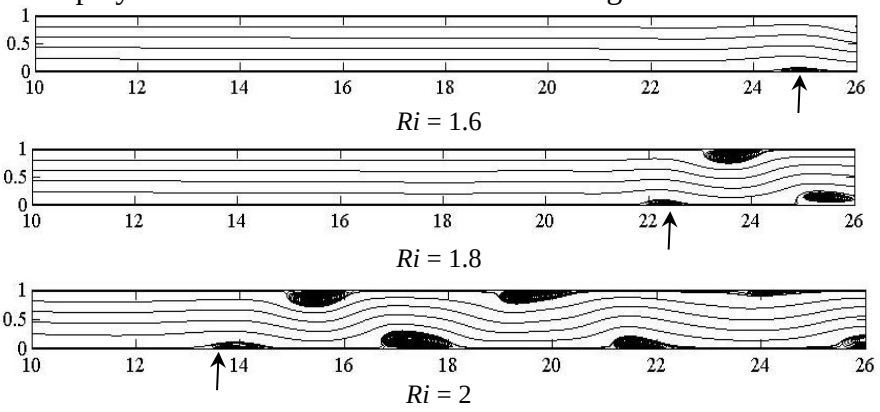

Fig. 7. Position of convective cells for different Richardson numbers at φ = 10%.

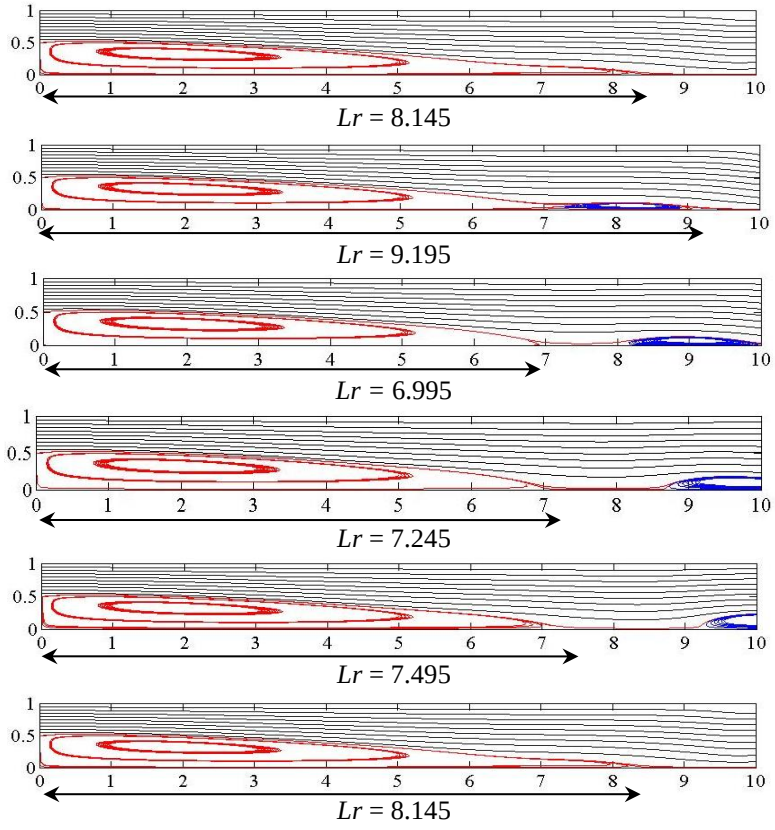

Fig. 8. Transient developments of streamlines for *Ri* = 2.2 at equal interval times (φ = 10%)

for different concentration of nanoparticles. As it can be seen, the reattachment length increases monotonously with the increasing *Ri* for all the volume fractions considered in this study and decreases as the volume fraction increases for a fixed

value of *Ri*. For each value of φ, numerical results show that *Lr* varies linearly with respect to the Richardson number. Using the least-square method for all the computed values, the following expressions may be derived:

For φ = 0% and $0 \le Ri \le 1.10$: $Lr = 2.67\,Ri + 3.78$ (15-1)

For φ = 5% and $0 \le Ri \le 1.55$: $Lr = 2.36\,Ri + 3.48$ (15-2)

For φ = 10% and $0 \le Ri \le 2.00$: $Lr = 1.91\,Ri + 3.31$ (15-3)

For φ = 15% and $0 \le Ri \le 2.40$: $Lr = 1.58\,Ri + 3.00$ (15-4)

For φ = 20% and $0 \le Ri \le 2.85$: $Lr = 1.24\,Ri + 2.79$ (15-5)

These correlations have a maximum deviation of about 2.5% from the computed values.

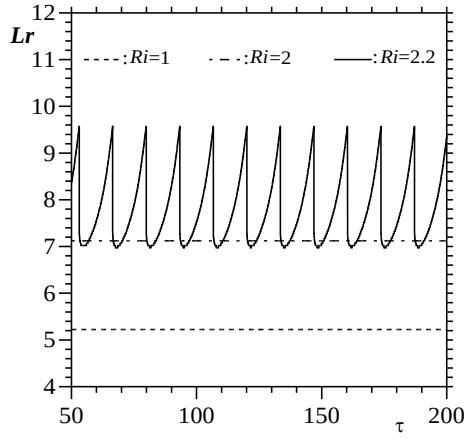

Fig. 9. Time signal of reattachment length *Lr* for different Richardson numbers at φ = 10%

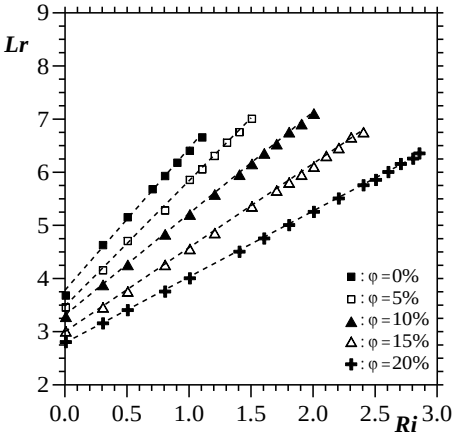

Fig. 10. Effect of nanoparticles volume fraction φ on variation of *Lr* with *Ri*

Isotherm contours are depicted in Fig. 11 for *Ri* = 0.5 at different values of φ. The tightening of the isotherms near the horizontal walls is observed by increasing the nanoparticles concentration. This causes the thinning of the thermal boundary layer which tremendously increases the heat transfer rate. Indeed, a close glance at Fig.12 presenting the Nusselt number distribution at the upper and the lower walls reveals a clear increase in the Nusselt number observed when increasing the nanoparticles volume fraction. This behavior was also observed by Abu-Nada [15] who showed that the increase in the Nusselt number is due to the increase in the inertial forces and the effective thermal conductivity.

Figure 13 shows the variation of the time and space-averaged Nusselt number $\overline{Nu}$ at the horizontal walls with the Richardson number for different concentrations of nanoparticles. We note that $\overline{Nu}$ is evaluated as follows:

$$\overline{Nu} = \frac{1}{\tau_2 - \tau_1} \int_{\tau_1}^{\tau_2} Nu_{av}\, d\tau \qquad (17)$$

where the time interval ($\tau_2 - \tau_1$) is large compared to the period of oscillations and usually chosen as an integer multiple of period oscillations. According to this figure, it is observed that the ranges within which buoyancy forces

have a negligible effect on the heat transfer are characterized by a slight variation in $\overline{Nu}$. These ranges, where the forced convection is dominant, extend with increasing φ. For each nanoparticle volume fraction under investigation, the computations show that the heat flux exchanged between the flow and the horizontal walls was affected by the buoyancy term when the Richardson number exceeds the value of Ri_{cr} All the curves show a remarkable increase beyond this value, indicating the high contribution of the buoyancy term on the increment of the heat transfer. Therefore, the mixed convection regime occurs beyond Ri_{cr}. For example, for φ = 10%, the exchange of heat transfer increased by 146% and 131% at the lower and upper walls respectively when we pass from Ri_{cr} to Ri_l. As expected, this significant increase is caused by the presence of the convective cells generated near the horizontal walls. As shown in Fig. 14, these convective cells provide the best mixing of hot fluid with cold fluid and, consequently, the highest heat transfer rate. Referring back to Fig. 13 again, when the flow is steady ($Ri < Ri_{cr}$), and contrarily to what was observed at the upper wall, a slight decrease in $\overline{Nu}$ was noted at the lower wall when increasing *Ri*. In fact, this decrease is attributed by the primary recirculation zone which turns in place and grows in size behind the facing step when *Ri* increases, acting as a barrier against the heat transfer from the hot lower wall to the flow. When *Ri* exceeds Ri_{cr}, the presence of the convective cells prevails this decrease and further improves the heat transfer.

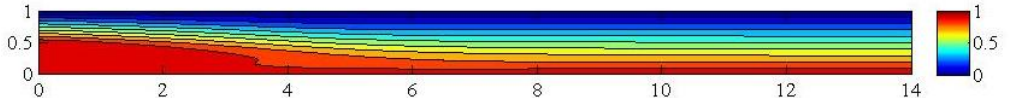

(a): φ = 0%

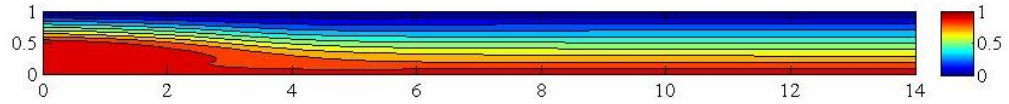

(c): φ = 10%

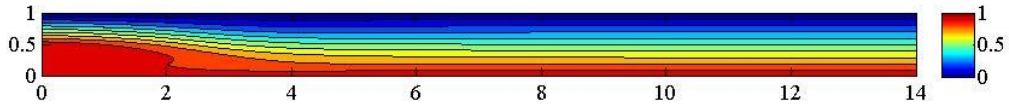

(c): φ = 20%

Fig. 11. Isotherm contours for different nanoparticles volume fractions at *Ri* = 0.5

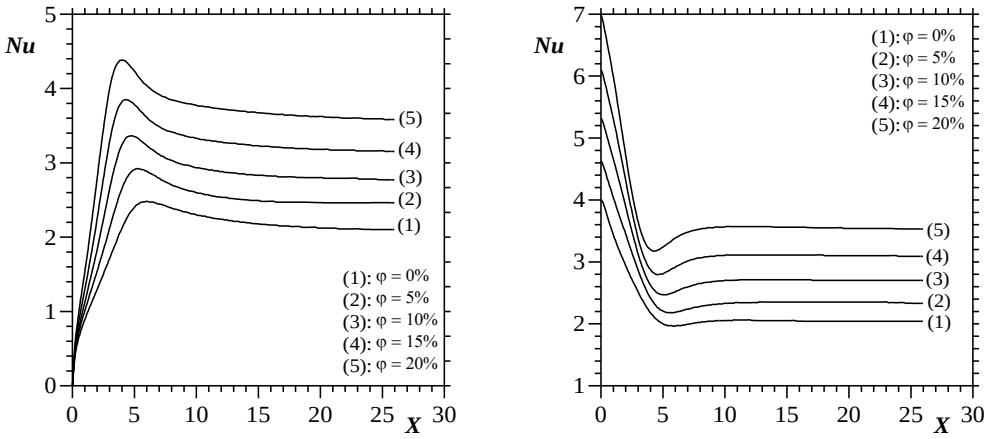

(a) : Lower wall (a) : Upper wall

Fig. 12. Local Nusselt distribution for different nanoparticles volume fractions at Ri = 0.5

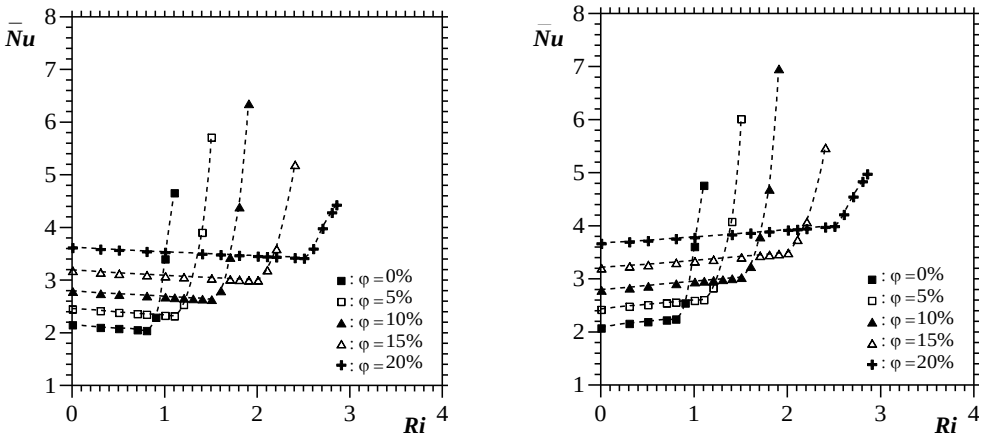

(b) : Lower wall (b) : Upper wall

Fig. 13. Effect of volume fraction φ on variation of $\overline{Nu}$ with Ri

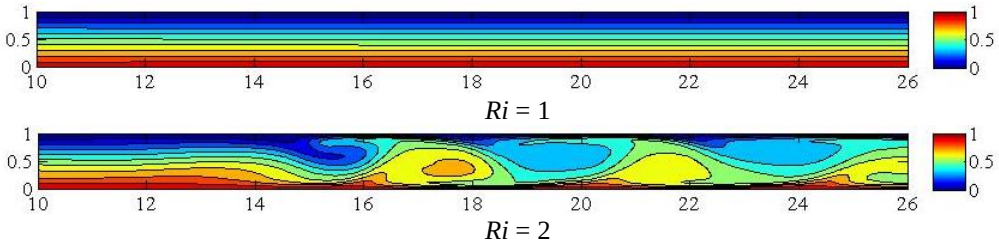

Ri = 1

Ri = 2

Fig. 14. Isotherm contours for two Richardson numbers either side of Ri_{cr}=1.55

5. Conclusions

Numerical study of the buoyancy effect on the flow pattern and heat transfer over a backward-facing step using *copper-water* nanofluid has been performed for

different nanoparticules volume fraction. Over a range of Richardson number *Ri* up to 2.85 and a volume fraction of nanoparticles φ from 0% to 20%, the obtained results in this study can be summarized as follows:

*) The critical Richardson number Ri_{cr}, characterizing the onset of convective cells near the horizontal walls, increases with the volume fraction φ. It can be correlated by the following relationship: $Ri_{cr} = 8.6\ \varphi + 0.8$

*) For different Richardson numbers and volume fraction of nanoparticles considered in this study, the reattachment length *Lr* can be correlated by the relationship: $Lr = a\ Ri + b$

The values of the coefficients "*a*" and "*b*" are given by equation (15) for different φ.

*) For a fixed Richardson number, the heat transfer exchanged between the horizontal walls and the flow increases by increasing the nanoparticles volume fraction and this enhancement is far more obvious when further increasing the nanoparticles concentration.

*) For each nanoparticle volume fraction under investigation, the buoyancy force plays a major role in increasing the heat transfer when the Richardson number exceeds Ri_{cr}.

R E F E R E N C E S

[1] *B.F. Armaly, F. Durst, J.C.F. Pereira, B. Schönung*, Experimental and theoretical investigation of backward-facing step flow, J. Fluid Mech., **vol.** 127, 1983, pp. 473–496.

[2] *J. Kim and P. Moin*, Application of a fractional-step method to incompressible Navier-Stokes equations, J. Computational Physics, **vol.** 59, 1985, pp. 308–323.

[3] *D.K. Gartling*, A test problem for outflow boundary condition-Flow over a backward- facing step, International Journal for Numerical Methods in Fluids, **vol.** 11, 1990, pp. 953–967.

[4] *D. Barkeley, M.G. Gomes, R.D. Henderson*, Three-dimensional instability in flow over a backward-facing step, J. Fluid Mech, **vol.** 473, pp. 2002 167-190.

[5] *H.I. Abu-Mulaweh*, A review of research on laminar mixed convection flow over backward and forward-facing steps, Int. J. Therm. Sci., **vol.** 42, 2003, pp. 897–909.

[6] *M. Ramsak and L.A. Skerget*, Subdomain boundary element method for high-Reynolds laminar flow using stream function–vorticity formulation, Int. J. Num. Meth. Fluids, **vol.** 46, 2004, pp. 815–847.

[7] *C.E. Tinney and E.L.S. Ukeiley*, A study of a 3-D double backward-facing step, Experiments in Fluids, **vol.** 47, 2009, pp. 427–439

[8] *Y. Xuan and Q. Li*, Investigation on convective heat transfer and flow features of nanofluids, Journal of Heat Transfer, **vol.** 125, 2003, pp. 151–155.

[9] *Y. Ding, H. Chen, L. Wang, C. Yang, Y. He, W. Yang, W.P. Lee, L. Zhang, L., R. Huo*, Heat transfer intensification using nanofluids, Journal of particle and Powder, **vol.** 25, 2007, pp. 23-38.

[10] *S. Kakaç and A. Pramuanjaroenkij*, Review of convective heat transfer enhancement with nanofluids, Int. J. Heat and Mass Transfer, **vol.** 52, 2009, pp. 3187-3196.

[11] *G. Ramesh and N.K. Prabhu*, Review of thermo-physical properties, wetting and heat transfer characteristics of nanofluids and their applicability in industrial quench heat treatment, Nanoscale Res. Lett., **vol.** 6, 2011, pp. 334.

[12] *R. Saidur, K.Y. Leong, H.A. Mohammad*, A review on applications and challengers of nanofluids, Renew. Sustain. Energy Rev., **vol.** 15, 2011, pp. 1646-1668.

[13] *T. Hung and W. Yan*, Enhancement of thermal performances in double-layered microchannel heat sink with nanofluids, Int. J. Heat Mass Transfer, **vol.** 55, 2012, pp. 3225-3238.

[14] *A.M. Hussein, K.V. Sharma, R.A. Bakar, K. Kadirgama*, A review of forced convection enhancement and hydrodynamic characteristics of a nanofluid, Renew Sustain Energy Rev. **vol.** 29, 2014, pp. 734-743.

[15] *E. Abu-Nada*, Application of nanofluids for heat transfer enhancement of separated flows encountered in a backward-facing step, Int. J. Heat and Fluid Flow, **vol.** 29, 2008, pp. 242–249.

[16] *A.A. Al-aswadi, H.A. Mohammed, N.H. Shuaib, A. Campo*, Laminar forced convection flow over a backward-facing step using nanofluids, Int. Comm. in Heat and Mass Transfer, **vol.** 37, 2010, pp. 950–957.

[17] *A.Sh. Kherbeet, H.A. Mohammed, B.H. Salman*, The effect of nanofluids flow on mixed convection heat transfer over micro scale backward-facing step, Heat and Mass Transfer, **vol.** 55, 2012, pp. 5870–5881.

[18] *H.A. Mohammed, A.A. Al-aswadi, H. Abu-Mulaweh, N.H. Shuaib*, Influence of nanofluids on mixed convective heat transfer over a horizontal backward-facing step, Heat Transfer – Asian Res, **vol.** 40, 2011, pp. 287–307.

[19] *H.A. Mohammed, A.A. Al-aswadi, M.Z. Yusoff, R. Saidur***,** Buoyancy-assisted Mixed convective flows over backward-facing step in a vertical duct using various nanofluids, Thermophysics and Aeromechanics, **vol.** 19, 2012, pp 33–52.

[20] *M. Saffari Pour and S.A. Gandjalikhan Nassab*, Numerical investigation of forced laminar convection flow of nanofluids over a backward-facing step under bleeding condition, Journal of Mechanics, **vol.** 28, 2012, pp. 7-12.

[21] *H.C. Brinkman*, The viscosity of concentrated suspensions and solutions, Journal of Chemical Physics, **vol.** 20, 1952, pp. 571–581.

[22] *K. Khanafer, K. Vafai, M. Lightstone*, Buoyancy-driven heat transfer enhancement in a two dimensional enclosure utilizing nanofluids, Int. J. Heat and Mass Transfer, **vol.** 46, 2003, pp. 3639–3653.

[23] *A. Sohankar, C. Norberg, L. Davidson*, Low-Reynolds number flow around a square cylinder at incidence: Study of blockage, onset of vortex shedding and outlet boundary condition, Int. J. for Numerical Methods in Fluids, **vol.** 26, 1998, pp. 39-56.

[24] *H. Abbassi, S. Turki, S. Ben Nasrallah*, Channel flow bluff-body: outlet boundary condition, vortex shedding and effects of buoyancy, Computational Mechanics, **vol.** 28, 2002, pp. 10-16.

[25] *S.V. Patankar*, Numerical heat transfer and fluid flow, Series in Computational Method in Mechanics and Thermal Sciences, Mac Graw Hill, New York, 1980.

[26] *S. Turki, and G. Lauriat*, Thermal convection of non-Newtonian fluids in enclosures, AIAA/ASME, Thermophysics and Heat Transfer Conference, 1990, pp. 165-170.